AD-A159 548 NUMERICAL APPROXIMATION OF THE TOTAL DRAG OF A BODY IN A TUBE(U) PENNSYLVANIA STATE UNIV UNIVERSITY PARK APPLIED RESEARCH LAB K C KAUFMAN 25 JUN 85 1/1

UNCLASSIFIED ARL/PSU/TM-85-108 N00024-79-C-6043 F/G 20/4 NL

END

FILMED

DTIC

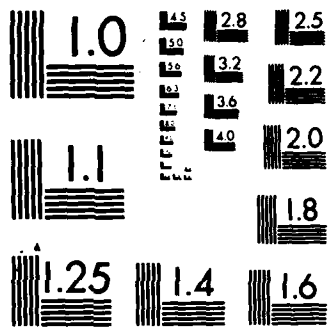


MICROCOPY RESOLUTION TEST CHART
NATIONAL BUREAU OF STANDARDS-1963-A

2

AD-A159 548

# NUMERICAL APPROXIMATION OF THE TOTAL DRAG OF A BODY IN A TUBE

K. C. Kaufman

Technical Memorandum
File No. TM 85-108
25 June 1985
Contract N00024-79-C-6043

Copy No. 2

The Pennsylvania State University
Intercollege Research Programs and Facilities
APPLIED RESEARCH LABORATORY
Post Office Box 30
State College, Pa. 16804



NAVY DEPARTMENT

NAVAL SEA SYSTEMS COMMAND

2

NUMERICAL APPROXIMATION OF THE
TOTAL DRAG OF A BODY IN A TUBE

K. C. Kaufman

Technical Memorandum
File No. TM 85-108
25 June 1985
Contract N00024-79-C-6043

Copy No. 2

The Pennsylvania State University
Intercollege Research Programs and Facilities
APPLIED RESEARCH LABORATORY
Post Office Box 30
State College, PA 16804

Approved for Public Release

NAVY DEPARTMENT

NAVAL SEA SYSTEMS COMMAND

UNCLASSIFIED

SECURITY CLASSIFICATION OF THIS PAGE (When Data Entered)

| REPORT DOCUMENTATION PAGE | | READ INSTRUCTIONS BEFORE COMPLETING FORM |
|---|---|---|
| 1. REPORT NUMBER<br>TM 85-108 | 2. GOVT ACCESSION NO.<br>AD-A159548 | 3. RECIPIENT'S CATALOG NUMBER |
| 4. TITLE (and Subtitle)<br>NUMERICAL APPROXIMATION OF THE TOTAL DRAG OF A BODY IN A TUBE | | 5. TYPE OF REPORT & PERIOD COVERED<br>Technical Memorandum |
| | | 6. PERFORMING ORG. REPORT NUMBER |
| 7. AUTHOR(s)<br>K. C. Kaufman | | 8. CONTRACT OR GRANT NUMBER(s)<br>N00024-79-C-6043 |
| 9. PERFORMING ORGANIZATION NAME AND ADDRESS<br>Applied Research Laboratory<br>The Pennsylvania State University<br>State College, PA 16804 | | 10. PROGRAM ELEMENT, PROJECT, TASK AREA & WORK UNIT NUMBERS |
| 11. CONTROLLING OFFICE NAME AND ADDRESS<br>Naval Sea Systems Command, Code NSEA 63R-31<br>Department of the Navy<br>Washington, DC 20362 | | 12. REPORT DATE<br>25 June 1985 |
| | | 13. NUMBER OF PAGES<br>42 |
| 14. MONITORING AGENCY NAME & ADDRESS(if different from Controlling Office) | | 15. SECURITY CLASS. (of this report)<br>Unclassified |
| | | 15a. DECLASSIFICATION/DOWNGRADING SCHEDULE |

16. DISTRIBUTION STATEMENT (of this Report)

Approved for public release. Distribution unlimited.
Per NAVSEA - 12 September 1985.

17. DISTRIBUTION STATEMENT (of the abstract entered in Block 20, if different from Report)

18. SUPPLEMENTARY NOTES

19. KEY WORDS (Continue on reverse side if necessary and identify by block number)

body drag
body in a tube

20. ABSTRACT (Continue on reverse side if necessary and identify by block number)

A study is made of numerical methods to approximate the total drag coefficient of an axisymmetric body in a tube. An analytical relationship for the drag coefficient is obtained via a standard open system control volume analysis. This relationship is found to be difficult to apply numerically using available numerical tools, leading to an approximation of the drag coefficient by neglecting the tube wall skin friction and the

DD FORM 1473, 1 JAN 73 EDITION OF 1 NOV 65 IS OBSOLETE

UNCLASSIFIED

SECURITY CLASSIFICATION OF THIS PAGE (When Data Entered)

pressure distribution across the tube radius near the body tail. The resulting drag coefficient approximation, which accounts for tunnel blockage and horizontal buoyancy effects, is found to provide a good estimate to available experimental data for an unheated body. The approximation makes use of currently available numerical codes for axisymmetric inviscid and boundary layer flow. Numerically obtained drag distributions over a range of Reynolds numbers are compared with experimental drag data for the unheated laminar flow body in the Garfield Thomas 48-inch diameter water tunnel.

-1-

From: K. C. Kaufman

Subject: Numerical Approximation of the Total Drag of a Body in a Tube

Abstract: A study is made of numerical methods to approximate the total drag coefficient of an axisymmetric body in a tube. An analytical relationship for the drag coefficient is obtained via a standard open system control volume analysis. This relationship is found to be difficult to apply numerically using available numerical tools, leading to an approximation of the drag coefficient by neglecting the tube wall skin friction and the pressure distribution across the tube radius near the body tail. The resulting drag coefficient approximation, which accounts for tunnel blockage and horizontal buoyancy effects, is found to provide a good estimate to available experimental data for an unheated body. The approximation makes use of currently available numerical codes for axisymmetric inviscid and boundary layer flow. Numerically obtained drag distributions over a range of Reynolds numbers are compared with experimental drag data for the unheated laminar flow body in the Garfield Thomas 48-inch diameter water tunnel.

Acknowledgment: This work has been supported by the Naval Sea Systems Command, Code NSEA 63R-31.

## Table of Contents

## Nomenclature

| | |
|---|---|
| $A_b$ | maximum body cross-sectional area |
| $C_D$ | total drag coefficient |
| $C_f$ | tunnel wall skin friction coefficient |
| $C_p$ | pressure coefficient |
| $D$ | total body drag |
| $R_b$ | maximum body radius |
| $R_I$ | sting radius |
| $R_O$ | tunnel radius |
| $Re_L$ | reference Reynolds number |
| $Re_x$ | local Reynolds number |
| $p$ | fluid pressure |
| $p_B$ | sting base pressure |
| $r$ | radius coordinate |
| $u$ | axial velocity |
| $x$ | axial coordinate |
| $\rho$ | fluid density |
| $\Theta$ | momentum deficit area coefficient |
| $\tau$ | shear stress |

Subscripts:

| | |
|---|---|
| 1,2 | initial and final control surface stations |
| $\infty$ | conditions far upstream of the body |
| w | conditions at tunnel wall |

## List of Figures



## List of Tables

## Introduction

The problem of numerically approximating the total drag coefficient of a body of revolution in a tube requires the determination of the entire flow field about the body and body wake. An interacting boundary layer approach, where the outer inviscid flow is linked to the boundary layer on the body by an iterative technique, would be the most accurate method to accomplish this [1]. For flow in a tube, the boundary layer on the tube wall would also need to be considered, as well as regions of strong interaction between the inviscid and viscous layers in the tail region of the body. Regions of separated flow might also need to be treated.

Such an interacting boundary layer approach would require sophisticated and complex computational methods and codes which are not readily available. Since the most accurate methods are not available, it is reasonable to examine a simplified approach, especially if only an estimate is required, not a high accuracy solution. The simplified approach would seek the best possible approximation for the drag coefficient using available tools. This estimate of drag coefficient values would be useful before beginning an experimental test in a water tunnel where drag values are to be measured. The numerical estimate would provide a check for experimental data being gathered.

A study is made here to determine an accurate but simple method to numerically approximate the drag coefficient of a body of revolution in a tube when the body diameter is an appreciable fraction of the tube diameter. The system geometry considered is modeled on the heated laminar flow body operating in the Garfield Thomas 48-inch diameter water tunnel, e.g., Ref. [2]. The flow is assumed to be axisymmetric and incompressible, with no heat addition.

To begin the examination of the problem, a standard control volume approach is applied to the system. Numerical techniques for approximating the total drag coefficient of the body are then developed after considering the results of the control surface analysis. These approximations are applied to the laminar flow body geometry using currently available codes to obtain a drag coefficient variation with reference Reynolds number.

Drag Coefficient Analysis

In Ref. [3], a standard open control volume treatment of a body/sting combination in a tube is considered. The drag of the body is obtained by applying conservation of momentum to the system. This approach can also be applied with minor changes to a closed body with a displacement wake continuing downstream and out of the control surface. Refer to Appendix A for a detailed development of this analysis and to Figures 1 and 2 for system schematics of the body/sting and closed body systems, respectively.

The result of the control surface analysis for the body/sting combination, given in Appendix A by Eq. (A.8), is

$$C_D = \frac{4}{R_b^2}\left[\theta_2 - \frac{1}{2}\int_{\hat{R}_I}^{\hat{R}_0} C_{p_2}\hat{r}d\hat{r} - \frac{1}{2}\int_{\hat{R}_0}^{\hat{R}_I} C_{p_B}\hat{r}d\hat{r} - \frac{\hat{R}_0}{2}\int_{\hat{x}_1}^{\hat{x}_2} C_f d\hat{x}\right] \quad . \qquad (1)$$

Similarly, for the closed body,

$$C_D = \frac{4}{R_b^2}\left[\Theta_2 - \frac{1}{2}\int_{0}^{\hat{R}_0} C_{p_2}\hat{r}d\hat{r} - \frac{\hat{R}_0}{2}\int_{\hat{x}_1}^{\hat{x}_2} C_f d\hat{x}\right] \qquad (2)$$

Note: Carets (^) indicate normalized quantities. The maximum body radius is the reference length.

[see Eq. (A.11)]. The main difference between Eqs. (1) and (2) is the base pressure term included in Eq. (1) due to the use of the sting mount. The base pressure is often corrected for in experimental procedures. This practice is assumed to be used here, eliminating the need for a correction in the analysis. Then Eq. (1) becomes

$$C_D = \frac{4}{R_b^2}\left[\Theta_2 - \frac{1}{2}\int_{\hat{R}_I}^{\hat{R}_0} C_{p_2}\hat{r}d\hat{r} - \frac{\hat{R}_0}{2}\int_{\hat{x}_1}^{\hat{x}_2} C_f d\hat{x}\right] \quad . \tag{3}$$

Comparing Eqs. (2) and (3) for the closed body and body/sting systems respectively, shows them to be almost identical except for the lower integration limit on the momentum deficit and pressure terms. This difference is due to the presence of the sting at Station 2 of the control surface.

There are three main terms in Eqs. (2) and (3) which contribute to the drag:

(1) momentum deficit area from the body boundary layer,

(2) pressure variation across the tube radius at Station 2 of the control surface, and

(3) skin friction on the tube or tunnel wall.

All three terms are integral quantities. The momentum deficit area is the dominant term and is dependent upon the boundary layer development on the body, particularly at the tail/sting region. The momentum deficit will vary corresponding to laminar or turbulent flow and attached or separated boundary layers.

The second term is an integral dependent on the pressure distribution across the tube radius at the final station of the control surface. This term becomes a factor in the drag calculation because the final station is taken only a small distance behind the body or back along the sting. The pressure across the tube at this point has not returned to the free-stream pressure as it would at a large distance downstream of the body. Extending the domain infinitely far downstream, however is not feasible. The pressure term is significantly influenced by the body boundary layer and wake and the tunnel boundary layer.

The tunnel wall skin friction term requires the calculation of the skin friction coefficient along the tunnel wall from Station $x_1$ to $x_2$, assuming it to be constant around the tunnel circumference at any one axial station. This term is included to account for the effects of the tunnel wall boundary layer. A standard procedure is to assume that the skin friction on the tunnel wall can be approximated by a skin friction relation for a turbulent flat plate boundary layer growing from Station $x_1$ [4]. Appendix B gives a detailed description of this skin friction approximation.

Examining the form of Eqs. (2) and (3), it is clear that this is the correct expression for the body drag in a tube. Young [5] gives the drag coefficient for an axisymmetric body in a free stream, with no other boundaries present, as

$$C_D = \frac{4\pi}{A} \Theta_\infty \tag{4}$$

where A is a reference area and $\Theta_\infty$ is the momentum deficit area far downstream of the body where the static pressure is equal to the freestream pressure. If the reference area is chosen to be the maximum cross-sectional area of the body, then

$$A = \pi R_b^2 \tag{5}$$

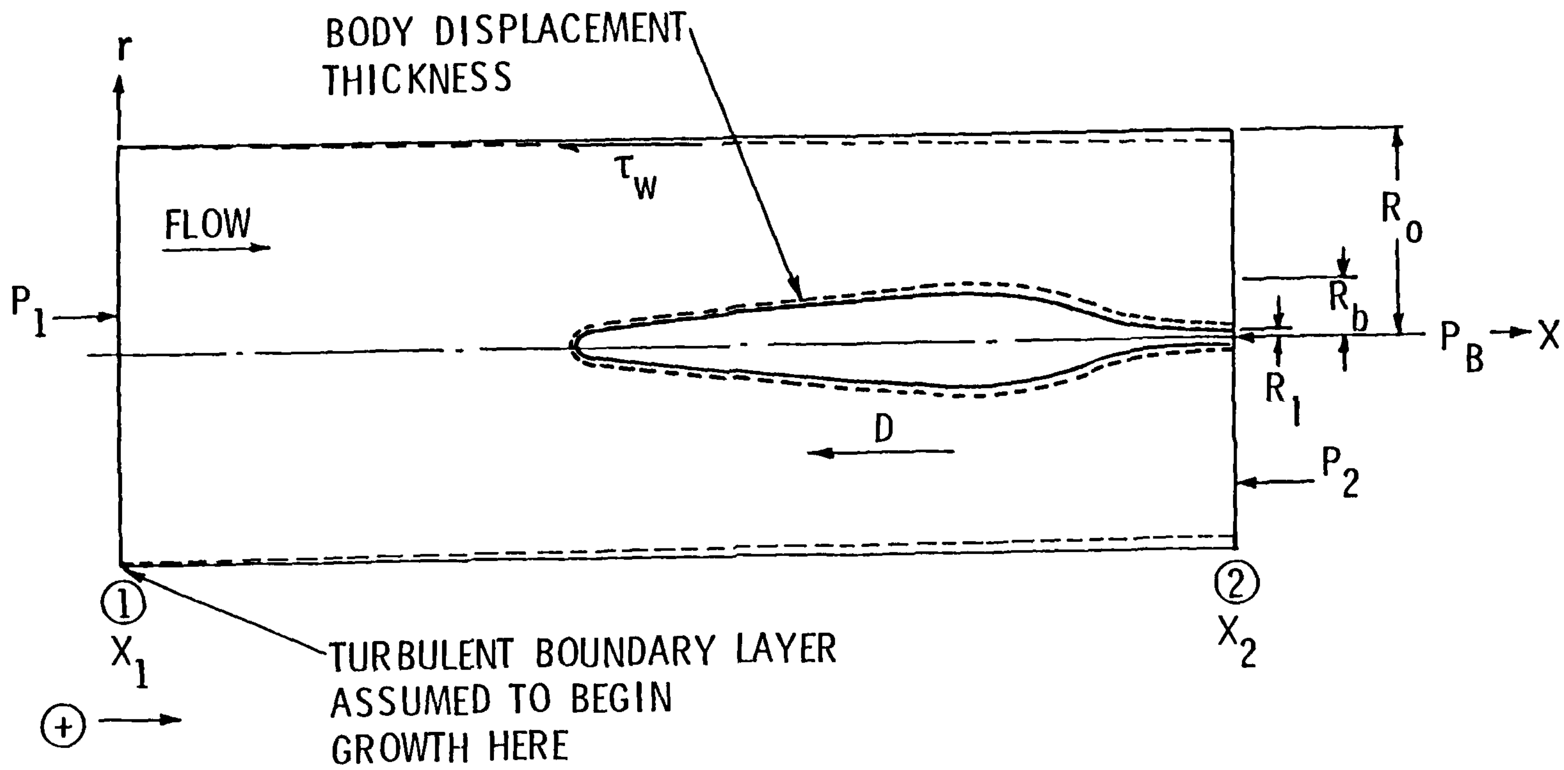


Figure 1. Open System Control Volume for the Body/Sting Configuration.

25 June 1985
KCK:lhz

Table 1. Drag Approximation Results for ARL Heated Laminar Flow Body

[Body with Sting]

| $Re_L$ | Inviscid Laminar | Inviscid Extrap. | Inviscid Turbulent | Inviscid Extrap. | Viscous Corrected Laminar | Viscous Corrected Extrap. | Viscous Corrected Turbulent | Viscous Corrected Extrap. |
|---|---|---|---|---|---|---|---|---|
| $5 \times 10^6$ | .03455 | ------ | .1331 | ------ | .03291 | .02655 | .1258 | .1031 |
| $1 \times 10^7$ | .02844 | ------ | .1176 | ------ | .02739 | .02198 | .1120 | .09067 |
| $2 \times 10^7$ | .02471 | ------ | .1049 | ------ | .02397 | .01911 | .1005 | .08054 |
| $3 \times 10^7$ | .02323 | ------ | .09845 | ------ | .02262 | .01795 | .09456 | .07538 |
| $4 \times 10^7$ | .02239 | ------ | .09432 | ------ | .02185 | .01728 | .09084 | .07216 |
| $5 \times 10^7$ | .02182 | ------ | .09136 | ------ | .02131 | .01682 | .08804 | .06974 |

[Body with Tail]

| $Re_L$ | Inviscid Laminar | Inviscid Extrap. | Inviscid Turbulent | Inviscid Extrap. | Viscous Corrected Laminar | Viscous Corrected Extrap. | Viscous Corrected Turbulent | Viscous Corrected Extrap. |
|---|---|---|---|---|---|---|---|---|
| $5 \times 10^6$ | .04011 | .02441 | ------ | ------ | .03972 | .02650 | .1345 | .1023 |
| $1 \times 10^7$ | ------ | ------ | .1352 | .08325 | ------ | ------ | .1275 | .08977 |
| $2 \times 10^7$ | ------ | ------ | ------ | ------ | ------ | ------ | .1197 | .07967 |
| $3 \times 10^7$ | .02800 | .01694 | .1183 | .07056 | .02701 | .01796 | .1125 | .07471 |
| $5 \times 10^7$ | .02618 | .01596 | .1094 | .06586 | .02537 | .01682 | .1042 | .06960 |

References


1. Davis, R. T. and M. J. Werle, "Progress on Interacting Boundary Layer Computations at High Reynolds Number," Numerical and Physical Aspects of Aerodynamic Flows, T. Cebeci (editor), Springer-Verlag, New York, pp. 187-210 (1982).

2. Lauchle, G. C. and G. B. Gurney, "Laminar Boundary Layer Transition on a Heated Underwater Body," J. Fluid Mech. 144:79-101 (1984).

3. Hoffman, G. H., Private Communication (29 October 1982).

4. Lauchle, G. C., "Horizontal Buoyancy Effects on the Pressure Distribution of a Body in a Duct," Journal of Hydronautics 13(2):61-67 (April 1979).

5. Young, A. D., "Calculation of the Total and Skin Friction Drags of Bodies of Revolution at Zero Incidence," ARC R and M NO. 1874 (April 1939).

6. Schlichting, H., Boundary Layer Theory, 6th Edition, McGraw-Hill, New York, pp. 635-640 (1979).

7. Hoffman, G. H., "A Modified Displacement-Body Method for Treating the Axisymmetric Strong-Interaction Problem," J. Ship Research 24:114-122 (June 1980).

8. Hoffman, G. H., Private Communcation (30 September 1982).

9. Hoffman, G. H., "A Method for Calculating the Flowfield in the Tail Region of a Body of Revolution," ARL/PSU TM 78-211, Applied Research Laboratory, The Pennsylvania State University (19 July 1978).

10. Hoffman, G. H., Private Communication (28 October 1982).

11. Ross, D. and J. H. McGinley, "Flow in Closed-Jet Working Sections," ORL Report NOrd 7958-282 (1954).

12. Lauchle, G. C., Private Communication (November 1984).

13. Hoffman, G. H., "A Frozen Vorticity Approach to the Axisymmetric Strong Interaction Problem," ARL/PSU TM 84-146, Applied Research Laboratory (14 September 1984).

## Concluding Remarks

A method for estimating the total drag coefficient of a body of revolution in a tube is developed. The method is simple in that it applies currently available tools and does not require an iteration process other than those in the automated numerical codes used. The approximation is found to provide reasonable results when compared with experimental data, and also yields a good trend to the data with variation of the Reynolds number.

The method, which is derived from a control surface analysis, is based upon obtaining an inviscid flow solution of the body geometry in a tube, yielding a pressure distribution over the body. Only axisymmetric, incompressible flows are considered. The pressure distribution is then corrected for viscous effects and used as input to a standard boundary layer code. The first order boundary layer solution provides a momentum deficit coefficient which is directly proportional to the approximated drag coefficient.

The approximation does not account for the skin friction on the tunnel wall or the pressure distribution near the body tail region, which is not equal to the freestream static pressure. These two terms are difficult to calculate accurately and tend to cancel each other since they are of opposite sign. To simplify the procedure, both are neglected in the approximation.

A possibility for future study could include applying a frozen vorticity approach like that developed by Hoffman [13] to the drag coefficient problem. This approach allows strong interaction effects to be considered and provides accurate results in the body tail region. The present method should also be further tested on other body shapes and flow conditions.

Figure 8 compares computed results with experimental hot and cold drag data for the heated laminar flow body [12]. Since only non-heated conditions were considered for the approximation, the cold data is of the most interest. The numerically calculated results provide a reasonable estimate of the cold experimental data, although the numerically approximated distribution is slightly lower than the experimental data, especially for the viscous corrected results. The computed results from the closed body geometry are compared with the experimental data, since the body/sting results display a greater slope as the Reynolds number increases, providing an unsatisfactory trend to the experimental data. The closed body results, however, provide a good comparison to the experimental data, if not an exact fit of the experimental points.

It is interesting to note that for the closed body cases computed, the inviscid results appear to match the experimental results better than the viscous corrected results. It is possible that the computed curves are shifted slightly down, since the momentum deficit coefficient could not be calculated into the near-wake. Further investigation is required to better explain this result. It should also be noted that the position of turbulent transition has an effect on the location of the drag curves. Since the transition locations of the experimental and computational results are not exactly matched, this will affect the comparison of the data.

Although not exactly fitting the available experimental data, the calculated results do provide a good estimate of the experimental data. This was the intention of the present study, to provide a reasonable approximation for experimental results. This would allow an estimate of the range of drag coefficient values to be available before testing is begun. This procedure appears to provide such an estimate.

The body geometry was used with two variations — a body/sting combination and a conical tail. See Figure 4 for a comparison of the tail region geometries. Drag coefficient distributions varying with Reynolds number were computed using both inviscid and viscous corrected pressure distributions. Two extreme cases of boundary layer transition were considered, with the turbulent boundary layer tripped at 7.5% or 77% of the body length. Reynolds numbers between 5 and 50 million are considered.

The results of the calculations are given in Table 1 and Figures 5, 6 and 7. The results for the body/sting combination are determined from $\Theta$ calculated at the $x_2$ station on the sting. These results are shown in Figure 5. For the body fitted with a conical tail, the boundary layer code indicates separation at approximately 95-96% of the body length for the Reynolds numbers considered. The drag coefficient is determined from the momentum deficit coefficient obtained at the last station before program failure. These results are shown in Figure 6 and all results are compared in Figure 7.

Figures 5, 6 and 7 also display extrapolated results. The extrapolated results were obtained by applying the $\Theta$ extrapolation procedure of ABL01 [9,10] to the body/sting and closed body results. For the body/sting combination, the extrapolation was applied to $\Theta_2$. For the closed body cases, the procedure was applied to the final $\Theta$ obtained before program termination. For both geometries, the drag curves obtained using extrapolation are drastically lower than the non-extrapolated results, especially when the turbulent boundary layer is tripped at 7.5% of the body length. These estimates are too low to be considered useful.

(5) With $\Theta$ calculated at Station $x_2$, the drag coefficient approximation is given by Eq. (6):

$$C_D = \frac{4}{R_b^2}\Theta_2 \quad .$$

(6) If the boundary layer program indicates separation near the tail end of the body, the value of $\Theta$ calculated at the last axial station before program failure may be used in Eq. (6). If the boundary layer code fails farther upstream than 95% of the body length, the drag estimate will most likely be poor.

Note that while the Douglas-Neumann results are independent of Reynolds number, both the horizontal buoyancy code and the axisymmetric boundary layer code require a reference Reynolds number to be input. The location of transition must also be input, although the boundary layer code can also empirically determine a transition location [8].

## Results

The drag coefficient approximation discussed above was applied to the geometry of the heated laminar flow body in a 48-inch diameter tube to model the Garfield Thomas 48-inch diameter water tunnel. The tube was extended 54 inches upstream of the body nose and a turbulent boundary layer was assumed to begin growth on the tunnel walls at that location. This distance includes the 17 inches of the test section ahead of the body nose as well as an additional 37 inches. The assumption is based on experimental data obtained by Ross [11].

Here, $u_m$ is the velocity at 54 units upstream of the body nose, as given by the DN program. For the case considered here, $u_0$ is unity. Equation (7) can be rearranged to yield

$$C_{p_{corrected}} = 1 - \frac{(1 - C_{p_u})}{(u_m/u_0)^2} \quad , \tag{8}$$

where

$$C_{p_u} = 1 - (\frac{u}{u_0}) \quad . \tag{9}$$

<u>Summary of Present Method Procedure</u>

(1) Obtain an inviscid pressure distribution for the desired body geometry in a tube via the Douglas-Neumann inviscid code.

(2) Correct the DN inviscid pressure distribution for the upstream velocity profile using Eq. (8) so that all velocities are based on a freestream velocity of unity.

(3) If desired, correct the inviscid DN pressure distribution from Step (2) for viscous effects using the horizontal buoyancy correction program [4].

(4) Determine the momentum deficit area coefficient $\Theta$ at Station $x_2$ using the axisymmetric boundary layer program, ABL01 [8].

(a) If the body is closed at the tail and $\Theta$ can be calculated into the near-wake, $\Theta_2$ can be extrapolated to infinity using an option of the ABL01 code.

(b) If the body continues into a sting, the momentum deficit coefficient should not be extrapolated. The value of $\Theta_2$ should be used for the drag coefficient estimate.

[see Figure 4] to observe which best fit the available experimental data. The investigation consisted of the following:

(1) An inviscid pressure distribution is obtained for the body of Ref. [2] mounted on a sting. The final control surface station, $x_2$, is located on the sting, 113.5 in. back from the body nose. The momentum deficit coefficient is computed to this station or the last station before separation.

(2) The inviscid pressure distribution of method (1) is corrected for viscous effects using the horizontal buoyancy program of Ref. [4]. The momentum deficit coefficient is calculated as in (1).

(3) An inviscid pressure distribution is obtained for the body fitted with a conical tail. The body length is 124.5 in. from nose to tail. The momentum deficit coefficient is computed into the near-wake or to the last station before separation and program failure.

(4) The inviscid pressure distribution of method (3) is corrected for viscous effects using the horizontal buoyancy program. The momentum deficit coefficient is calculated as in (3).

Note that the pressure coefficient distribution obtained from the DN code must be corrected for the upstream uniform velocity profile. As can be seen in Figure 3, the profile upstream of the body does not have a value of unity, on which subsequent calculations are based. The inviscid pressure distribution can be corrected using the relationship

$$C_{p_{corrected}} = 1 - \left(\frac{u}{u_0}\right)^2 \left(\frac{u_0}{u_m}\right)^2 \quad . \tag{7}$$

considering the canceling effect of pressure and friction terms. This leaves only the momentum deficit area term and a drag coefficient equation of the form

$$C_D = \frac{4}{R_b^2} \Theta_2 \quad . \tag{6}$$

Considering the calculation of the momentum deficit term, there are several options available. If the boundary layer does not separate and $\Theta$ can be calculated into the near-wake, then $\Theta_2$ can be extrapolated to $\Theta_\infty$ using the method detailed by Hoffman [9,10]. The DN code will provide an inviscid pressure distribution over the body, correcting for the inviscid blockage effects of the tunnel, with the horizontal buoyancy code [4] correcting the pressure distribution for viscous effects. The axisymemtric boundary layer code then provides the momentum deficit coefficient, $\Theta$, extrapolating $\Theta_2$ in the near-wake to $\Theta_\infty$.

If the boundary layer on the body separates, the boundary layer code will fail as the body skin friction approaches zero. This prevents the calculation of the momentum deficit area into the near-wake and the extrapolation to infinity. This was the case in the present study where the tail region configuration led to a severe adverse pressure gradient. This was true only for the case where the laminar flow body geometry was fitted with a conical tail. When the body is considered with a sting, the body does not close and a momentum deficit area at infinity can not be obtained.

Several approaches for obtaining a drag coefficient distribution with reference Reynolds number were attempted. The approaches included computations for the body fitted with a sting as well as a conical tail

Details of the Method

From the previous discussion, it is clear that accurate numerical approximation of Eqs. (2) or (3) would be difficult. Accurately determining the pressure coefficient integral term could probably only be accomplished with an interacting boundary layer approach or a full Navier-Stokes solution. For the skin friction term, only a rough approximation is readily available. Only the momentum deficit area can be calculated accurately and then only when the flow does not experience separation.

With the tools available, the axisymmetric boundary layer code, the Douglas-Neumann inviscid code, and a procedure which corrects for horizontal buoyancy effects [4], the most likely candidate for approximation of Eq. (2) would be to drop the pressure coefficient integral term. Assuming all three integrals are positive, this would appear to lead to a slight over-estimate. This is not the case, however; Figure 3 shows velocity profiles determined by the DN inviscid code at several streamwise stations. Near the tail of the body, the velocity between the body and the tunnel wall is approximately 5% greater than the freestream speed due to tunnel blockage effects. The pressure coefficient integral then becomes negative, with the situation exaggerated if the boundary layers on the body and tunnel, which effectively narrow the channel, are considered. The pressure and friction integrals would then tend to cancel each other.

With the above information in mind, the most logical approximation to make in the present analysis is to disregard both the pressure and friction terms. Estimating the drag using the momentum deficit and the friction term could lead to a significant underestimate of the drag coefficient, Such an approximation is the method of Young [5], which uses only the inviscid surface velocity for an integral .ethod, and does not account for separated regions. Since this method is well established and includes inaccuracies in the tail and wake region, it was not considered here.

The last term that needs to be considered is the pressure coefficient distribution across the tunnel radius at Station 2. This requires an accurate velocity distribution at the same location. The Douglas-Neumann code is presently available to calculate the inviscid flow over a body, including the blockage effect of the tunnel walls. The Douglas-Neumann (DN) code will provide a detailed velocity profile or "rake" across the tunnel at a specified station. This velocity profile is not dependent on the Reynolds number and is also independent of the state of development of the boundary layers on the body and tunnel walls. Because these effects are significant for an accurate result, the DN inviscid rake is insufficient for the present problem.

After considering the possibilities for determining each of the required terms for the control surface drag relationships, it is evident that with presently available methods, the options are severely limited, without the development of new methods. The pressure distribution term cannot be determined accurately and the skin friction term available is only an approximation. Only the momentum deficit area can be calculated with accuracy and then only when the boundary layer is non-separating. Since boundary layer separation is often quite probable, especially near trailing edges or tail regions, an accurate approximation of the drag coefficient is difficult. This was the case with the body geometry studied here. However, an estimate is still possible and the approximations attempted for this study are discussed in the following section.

layer as a turbulent flat plate boundary layer beginning at Station 1 [4,6]. For a more accurate estimate, the axisymemtric geometry of the tunnel wall would need to be considered. Only the flat plate estimate is considered here.

The momentum deficit area can be obtained using a standard axisymmetric boundary layer solution code, such as ABL01 which is available at ARL [7,8]. This code solves the first order boundary layer equations in finite difference form using a Newton iteration technique. Turbulent boundary layers are treated using an algebraic eddy viscosity model modified for extra rates of strain in the turbulent axisymmetric boundary layer.

For a non-separated boundary layer, ABL01 can determine $\Theta$ at the tail of the body, and using an extrapolation method [9,10], determine $\Theta_\infty$. Neither the boundary layer code nor the extrapolation include strong interaction effects present at the tail of the body where streamline curvature effects, as well as the abrupt transition from boundary layer to wake, become important. An iteration method which couples the boundary layer solution to the outer inviscid flow solution would account for most interaction effects at the tail of the body. An interacting boundary layer approach would not, however, include normal pressure gradient effects which are significant where streamline curvature is large [1].

Although the available boundary layer code, ABL01, works well for non-separated boundary layers, it fails when the wall shear approaches zero, indicating separation. If this is the case, a method capable of handling the separated regions must be developed, or approximations must be made which permit an approximate solution in this region, since separated regions will affect the required value of the momentum deficit coefficient.

and Eq. (4) has the same form as the first term in Eqs. (2) and (3). The two additional terms in these equations are present since

(1) the momentum deficit is not evaluated at an infinite distance downstream of the body, preventing the static pressure from returning to the freestream pressure, and

(2) the body is not positioned in a free stream, but inside a cylindrical tube which experiences friction with the fluid and also produces a blockage effect in the velocity distribution around the body.

The two additional terms present in the derived drag relationships correct for these effects.

The analytically determined equations for closed bodies or body/sting combinations are then correct as they stand. Methods to yield numerical results by evaluating these equations must now be developed and applied.

## Numerical Approach

### Preliminary Discussion

The drag coefficient equations discussed in the previous section, Eq. (2) for a closed body and Eq. (3) for a body/sting combination, are essentially identical except for changes in the lower integration limits. For clarity, the drag coefficient relation for the closed body will be considered primarily. Exceptions are noted for the body/sting case when necessary.

Three integral quantities in Eq. (2) must be evaluated to determine an accurate estimate of the drag coefficient. Appendix B describes an approximation which allows an analytical closed form evaluation of the skin friction term. This simplification treats the tunnel wall boundary

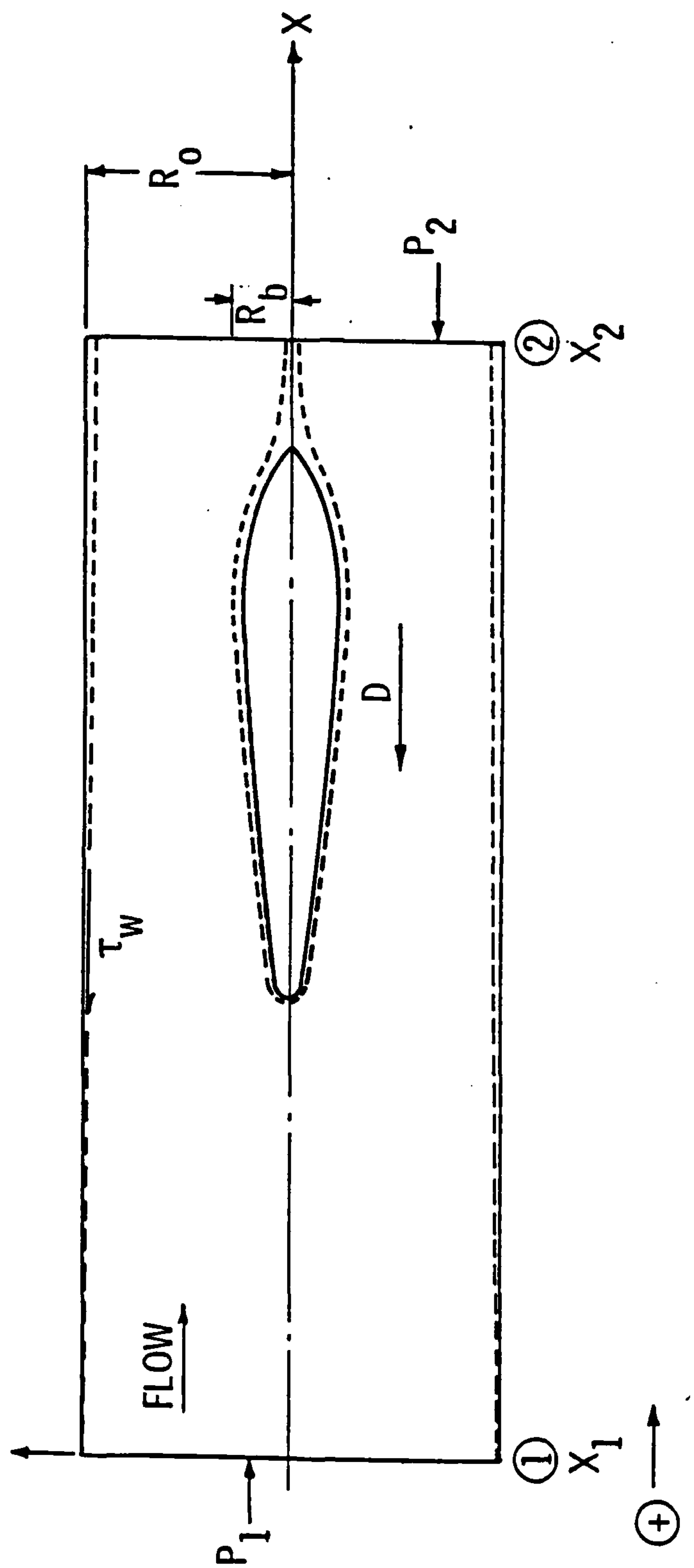


Figure 2. Open System Control Volume for the Closed Body Configuration.

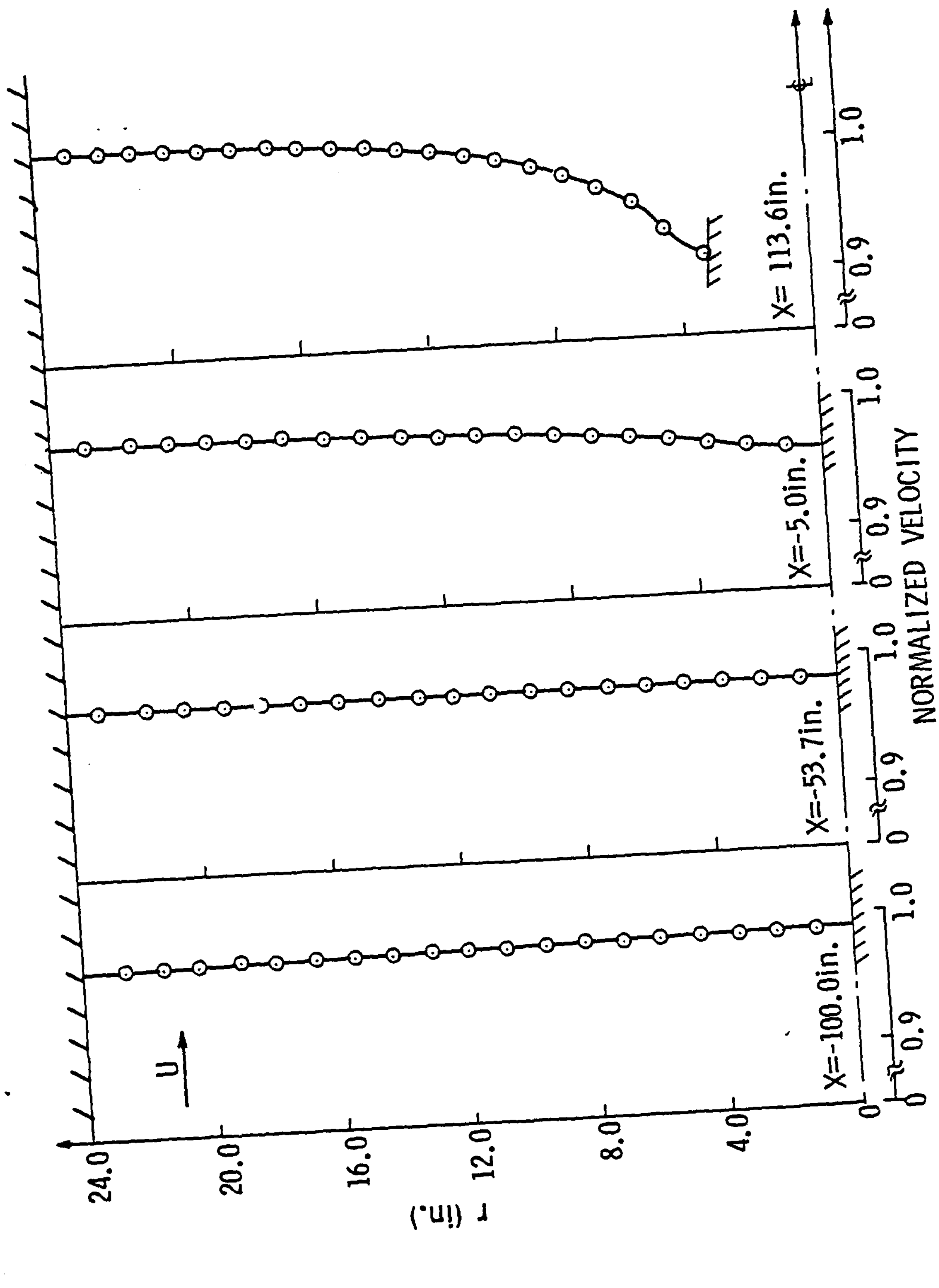


Figure 3. Normalized Velocity Profiles Obtained from the Douglas-Neumann Inviscid Code.

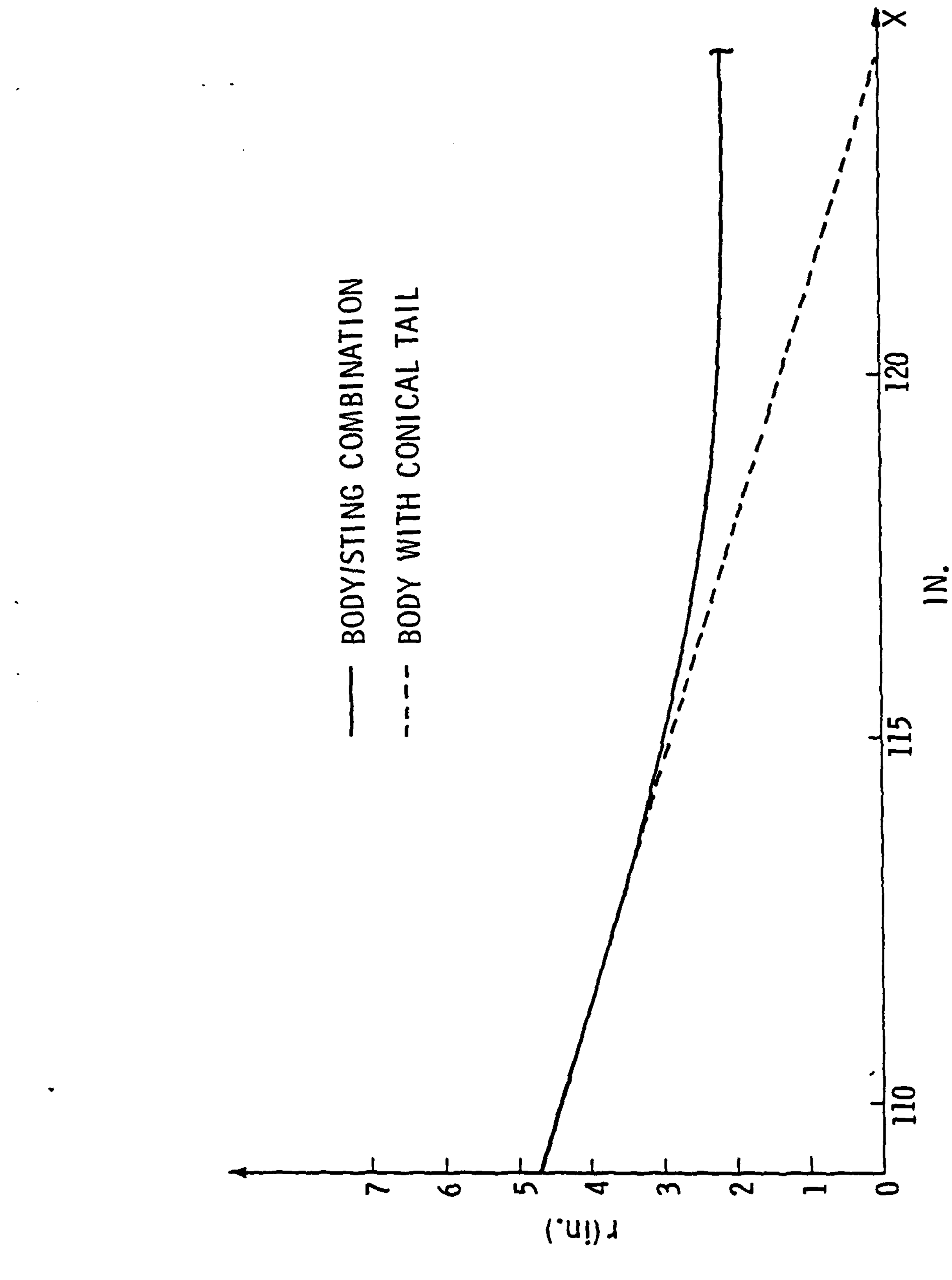


Figure 4. Comparison of Body/Sting and Conical Tail Geometry.

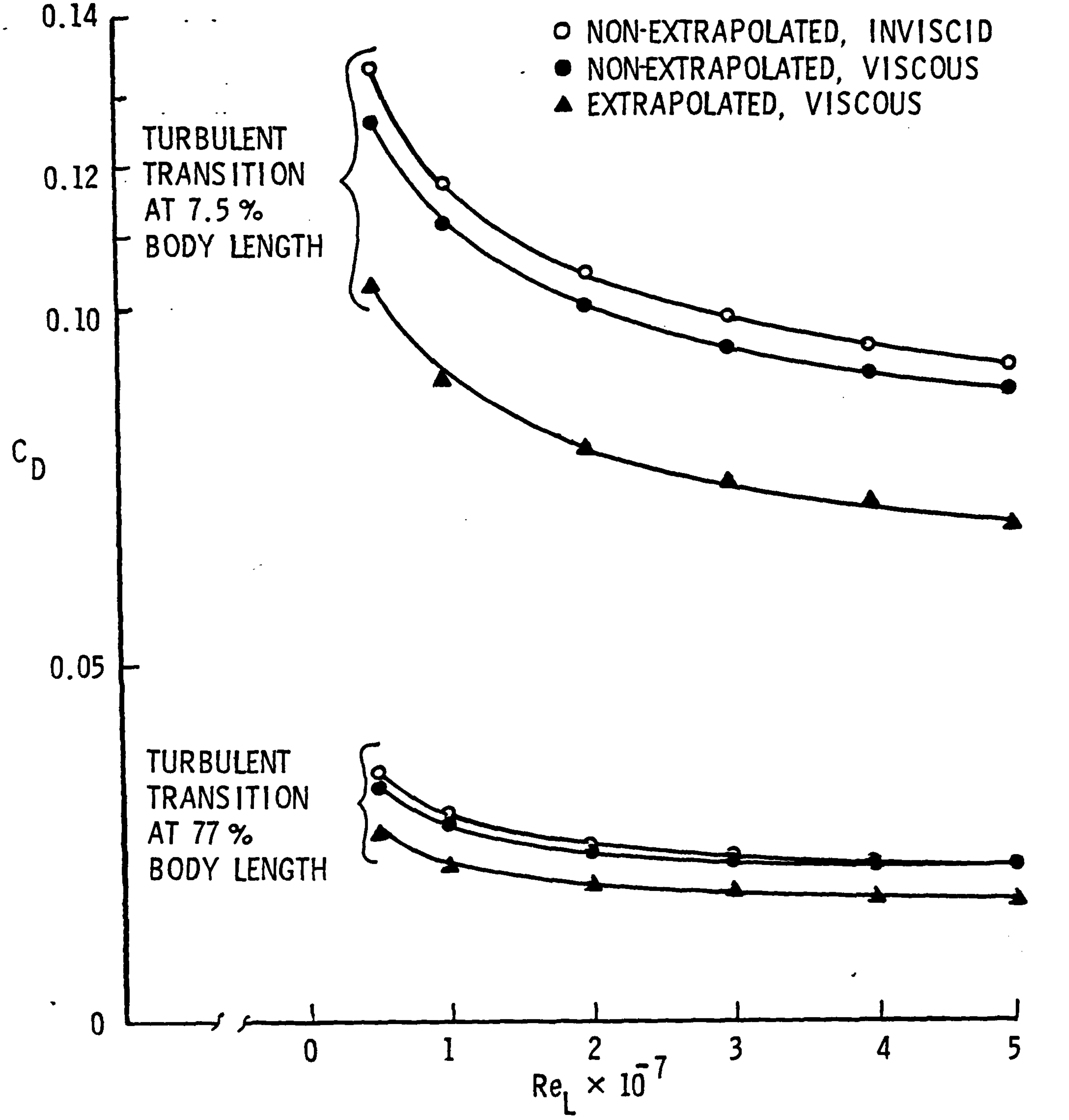


Figure 5. Drag Results for Laminar Flow Body with Sting.

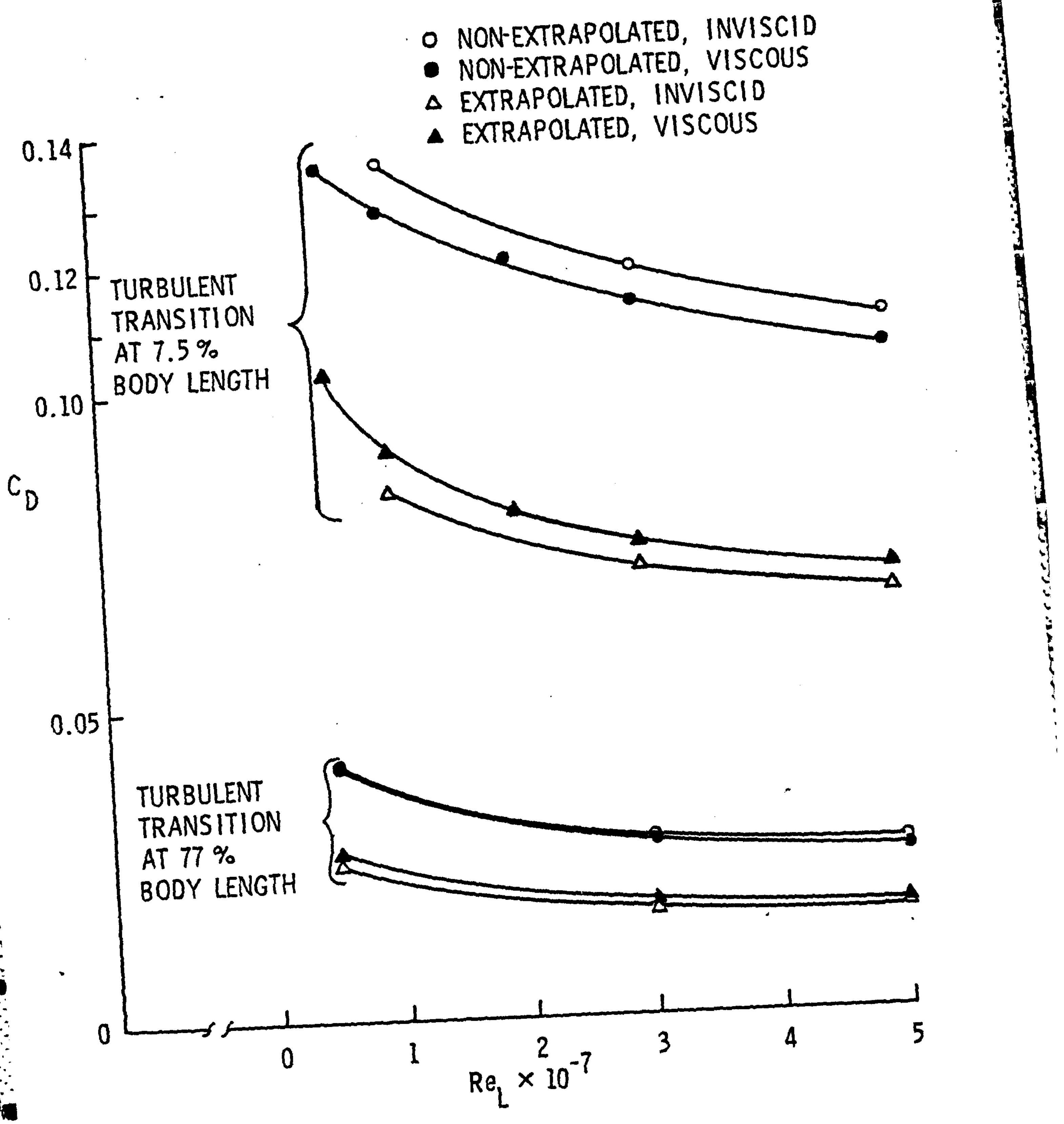


Figure 6. Drag Results for Laminar Flow Body with Conical Tail.

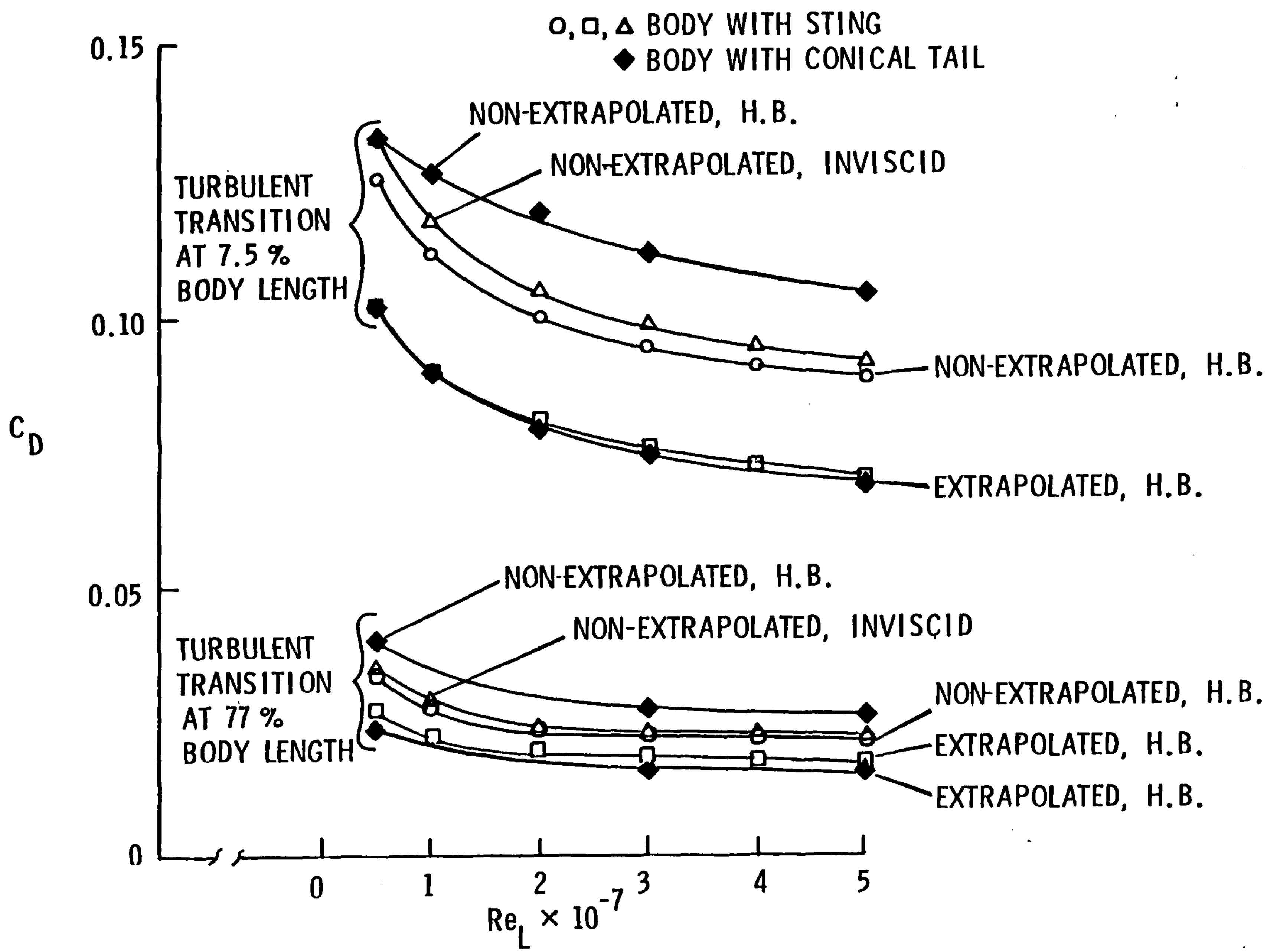


Figure 7. Comparisons for Laminar Flow Body Drag Approximations for Body/Sting and Closed Body Configurations.

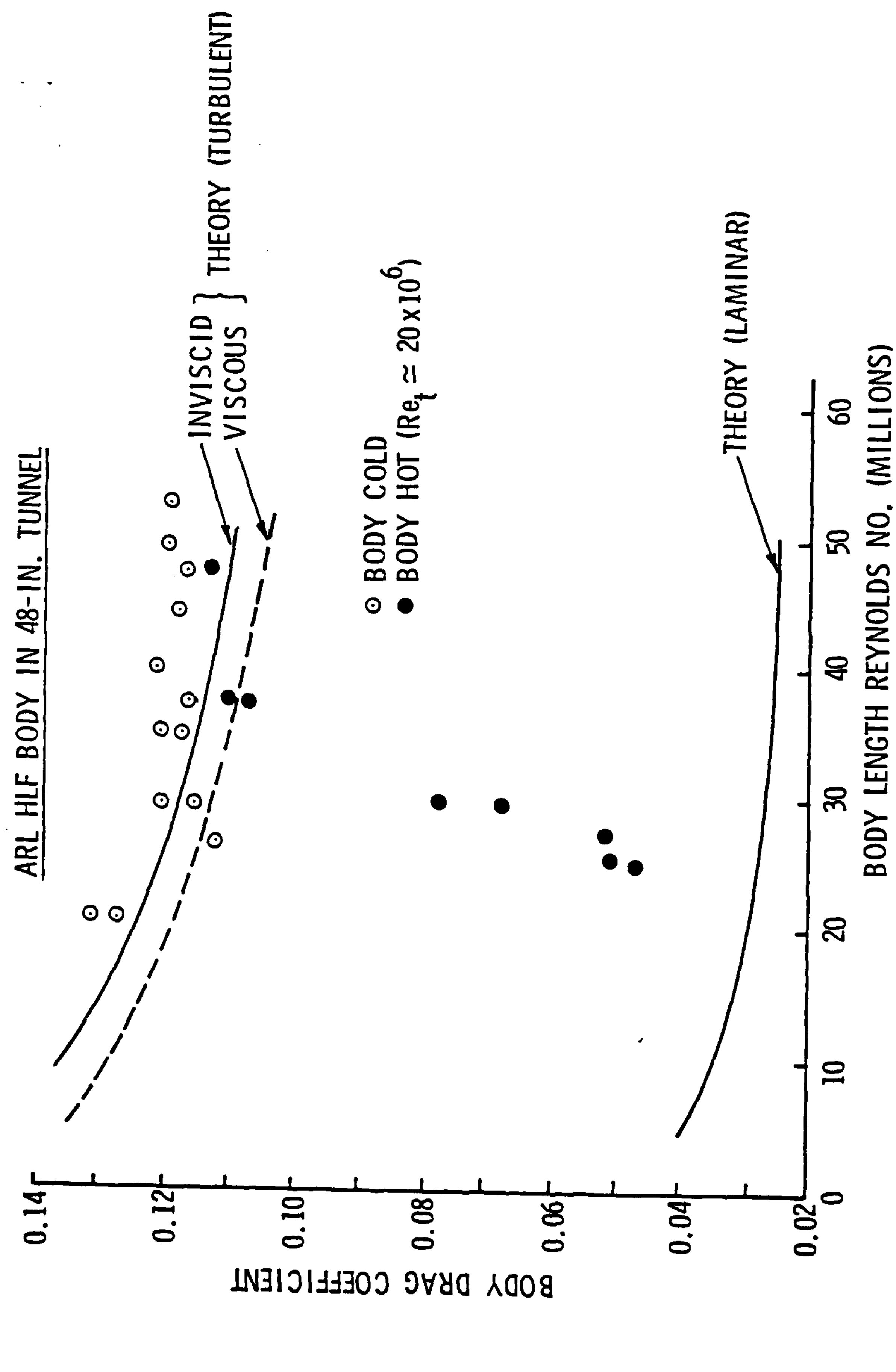


Figure 8. Comparison of Closed Body Drag Approximation Results with HLF Body Experimental Data.

## Appendix A

Consider the open system control volume for a body/sting combination shown in Figure 1. From conservation of momentum

(exterior forces on the fluid)

= (momentum out of C.V.) - (momentum into C.V) .

For the x-component of momentum

$$\int_0^{R_0} p_1(2\pi r dr) - \int_{R_I}^{R_0} p_2(2\pi r dr) - \int_0^{R_I} p_B(2\pi r dr) - \int_{x_1}^{x_2} \tau_w(2\pi R_0)dx - D$$

$$= \int_{R_I}^{R_0} \rho_2 u_2^2(2\pi r dr) - \int_0^{R_0} \rho_1 u_1^2(2\pi r dr) \quad . \tag{A.1}$$

From continuity

$$\int_{R_I}^{R_0} \rho_2 u_2(2\pi r dr) - \int_0^{R_0} \rho_1 u_1(2\pi r dr) = 0 \tag{A.2}$$

Multiplying Eq. (A.2) by the freestream velocity $u_\infty$,

$$\int_{R_I}^{R_0} \rho_2 u_2 u_\infty(2\pi r dr) - \int_0^{R_0} \rho_1 u_1 u_\infty(2\pi r dr) = 0 \quad . \tag{A.3}$$

Subtracting Eq. (A.3) from the RHS of Eq. (A.1) yields

$$\int_0^{R_0} p_1(2\pi r dr) - \int_{R_I}^{R_0} p_2(2\pi r dr) - \int_0^{R_I} p_B(2\pi r dr)$$

$$- \int_{x_1}^{x_2} \tau_w(2\pi R_0)dx - D = \int_{R_I}^{R_0} \rho_2 u_2^2(2\pi r dr)$$

$$- \int_{R_I}^{R_0} \rho_2 u_2 u_\infty(2\pi r dr) - \int_0^{R_0} \rho_1 u_1^2(2\pi r dr) + \int_0^{R_0} \rho_1 u_1 u_\infty(2\pi r dr) \quad .$$

Combining terms and dividing by $2\pi$, the equation becomes

$$- \int_{R_I}^{R_0} (p_2 - p_1) r dr - \int_0^{R_I} (p_B - p_1) r dr - \int_{x_1}^{x_2} \tau_w R_0 dx - \frac{D}{2\pi}$$

$$= \int_{R_I}^{R_0} \rho_2 u_2(u_2 - u_\infty) r dr - \int_0^{R_0} \rho_1 u_1(u_1 - u_\infty) r dr \quad .$$

Assuming that the flow is incompressible and $\rho_2 = \rho_1 = \rho_\infty$, divide by $\rho_\infty u_\infty^2 L$, where L is a reference length:

$$\frac{D}{2\pi\rho_\infty u_\infty^2 L} = -\int_{\hat{R}_I}^{\hat{R}_0} \frac{(p_2 - p_1)}{\rho_\infty u_\infty^2}\,\hat{r}d\hat{r} - \int_0^{\hat{R}_I} \frac{p_B - p_1}{\rho_\infty u_\infty^2}\,\hat{r}d\hat{r}$$

$$-\frac{R_0}{L}\int_{\hat{x}_1}^{\hat{x}_2} \frac{\tau_w}{\rho_\infty u_\infty^2}\,d\hat{x} + \int_{\hat{R}_I}^{\hat{R}_0} \frac{u_2}{u_\infty}\left(1 - \frac{u_2}{u_\infty}\right)\hat{r}d\hat{r} - \int_0^{\hat{R}_0} \frac{u_1}{u_\infty}\left(1 - \frac{u_1}{u_\infty}\right)\hat{r}d\hat{r} \tag{A.4}$$

where $\hat{R} = \frac{R}{L}$ , $\hat{x} = \frac{x}{L}$ , and $\hat{r} = \frac{r}{L}$. If Station $x_1$ is taken upstream so that $p_1 = p_\infty$ and $u_1 = u_\infty$, and defining the pressure, skin friction and momentum deficit area coefficients

$$C_p = \frac{p - p_\infty}{1/2\rho_\infty u_\infty^2} \tag{A.5a}$$

$$C_f = \frac{\tau_w}{1/2\rho_\infty u_\infty^2} \tag{A.5b}$$

and

$$\Theta_2 = \int_{\hat{R}_I}^{\hat{R}_0} \left(1 - \frac{u_2}{u_\infty}\right)\frac{u_2}{u_\infty}\,\hat{r}d\hat{r} \quad , \tag{A.5c}$$

then Eq. (A.4) becomes

$$\frac{D}{2\pi\rho_\infty u_\infty^2 L} = -\frac{1}{2}\int_{\hat{R}_I}^{\hat{R}_0} C_{p_2}\hat{r}d\hat{r} - \frac{1}{2}\int_0^{\hat{R}_I} C_{p_B}\hat{r}d\hat{r} - \frac{R_0}{2}\int_{\hat{x}_1}^{\hat{x}_2} C_f d\hat{x} + \Theta_2 \quad . \tag{A.6}$$

If the drag coefficient is redefined as

$$C_D = \frac{D}{1/2\rho_\infty u_\infty^2 A_b}$$

where $A_b = \pi R_b^2$. Then the drag coefficient relation, Eq. (A.6), can be written as

$$C_D = \frac{4}{R_b^2}\left[\Theta_2 - \frac{1}{2}\int_{\hat{R}_I}^{\hat{R}_0} C_{p_2}\hat{r}d\hat{r} - \frac{1}{2}\int_0^{\hat{R}_I} C_{p_B}\hat{r}d\hat{r} - \frac{\hat{R}_0}{2}\int_{\hat{x}_1}^{\hat{x}_2} C_f d\hat{x}\right] \quad . \tag{A.7}$$

This same procedure can be repeated for the closed body configuration in Figure 2. For the closed body system, the base pressure term is not required. The momentum equation in the x-direction is then

$$\int_0^{R_0} p_1(2\pi r dr) - \int_0^{R_0} p_2(2\pi r dr) - \int_{x_1}^{x_2} \tau_w(2\pi R_0)dx$$

$$- D = \int_0^{R_0} \rho_2 u_2^2(2\pi r dr) - \int_0^{R_0} \rho_1 u_1^2(2\pi r dr) \quad . \tag{A.8}$$

Continuity yields

$$\int_0^{R_0} \rho_2 u_2 (2\pi r dr) - \int_0^{R_0} \rho_1 u_1 (2\pi r dr) = 0 \tag{A.9}$$

Following the same manipulations as applied to the body/sting equations, the result for a closed body is

$$C_D = \frac{4}{R_b^2} \left[\Theta_2 - \frac{1}{2} \int_0^{\hat{R}_0} C_{p_2} \hat{r} d\hat{r} - \frac{\hat{R}_0}{2} \int_{\hat{x}_1}^{\hat{x}_2} C_f d\hat{x}\right] \tag{A.10}$$

where

$$\Theta_2 = \int_0^{\hat{R}_0} \left(1 - \frac{u_2}{u_\infty}\right) \frac{u_2}{u_\infty} \hat{r} d\hat{r} \quad .$$

The main assumptions involved in the above analysis are:

(1) The flow is incompressible.

(2) The flow is unheated.

(3) The flow is axisymmetric.

(4) The Station $x_1$ is taken a distance upstream of the body such that the conditions there are equal to the freestream conditions.

## Appendix B

One of the terms involved in the drag coefficient analysis is the integral of the tunnel wall skin friction from location $x_1$ to $x_2$. This integral has the form

$$C_{D_f} = \int_{\hat{x}_1}^{\hat{x}_2} C_f d\hat{x} \quad . \tag{B.1}$$

To avoid applying a complex boundary layer analysis to the tunnel wall, the determination of $C_{D_f}$ can be simplified by assuming the tunnel wall boundary layer behaves as a fully turbulent flat plate boundary layer, beginning at $x_1$. Then, well-known turbulent flat plate boundary layer relations can be applied. From Ref. [6]

$$C_f = 0.0592(Re_x)^{-1/5} \tag{B-2}$$

where $Re_x = \frac{u_\infty x}{\nu}$. Noting that

$$\frac{Re_x}{Re_L} = \left(\frac{u_\infty x}{\nu}\right)\left(\frac{\nu}{u_\infty L}\right) = \frac{x}{L} = \hat{x} \quad , \tag{B.3}$$

then

$$C_f = 0.0592(Re_L \hat{x})^{-1/5} \quad . \tag{B.4}$$

Substituting (B.4) into (B.1) yields

$$C_{D_f} = 0.0592 \, Re_L^{-1/5} \int_{\hat{x}_1}^{\hat{x}_2} \hat{x}^{-1/5} dx \quad ,$$

or

$$C_{D_f} = 0.074 \, Re_L^{-1/5} (\hat{x}_2^{4/5} - \hat{x}_1^{4/5}) \quad . \tag{B.5}$$

If the $\hat{x}_1$ location is taken as the origin, then

$$C_{D_f} = 0.074 \, Re_L^{-1/5} \, \hat{x}_2^{\,4/5} \quad . \tag{B.6}$$

DISTRIBUTION LIST FOR UNCLASSIFIED TECHNICAL MEMORANDUM 85-108,
by K. C. Kaufman, dated 25 June 1985

Defense Technical Information
Center
5010 Duke Street
Cameron Station
Alexandria, VA 22314
(Copies 1 through 6)

Commander
David W. Taylor Naval Ship
Research & Development Ctr.
Department of the Navy
Bethesda, MD 20084
Attn: M. J. Casarella
Code 1940
(Copy No. 7)

Commander
David W. Taylor Naval Ship
Research & Development Ctr.
Department of the Navy
Bethesda, MD 20084
Attn: T. T. Huang
Code 1542
(Copy No. 8)

Commander
David W. Taylor Naval Ship
Research & Development Ctr.
Department of the Navy
Bethesda, MD 20084
Attn: J. H. McCarthy
Code 1540
(Copy No. 9)

Dynamics Technology, Inc.
Suite 200
22939 Hawthorne Blvd.
Torrance, CA 90505
Attn: W. W. Haigh
(Copy No. 10)

Commander
Naval Sea Systems Command
Department of the Navy
Washington, DC 20362
Attn: Library
Code NSEA-09G32
(Copies 11 and 12)

Commander
Naval Sea Systems Command
Department of the Navy
Washington, DC 20362
Attn: T. E. Peirce
Code 63R-31
(Copy No. 13)

Commander
Naval Sea Systems Command
Department of the Navy
Washington, DC 20362
Attn: F. J. Romano
Code 63R
(Copy No. 14)

Director
Naval Research Laboratory
Washington, DC 20390
Attn: E. W. Hendricks
(Copy No. 15)

Director
Naval Research Laboratory
Washington, DC 20390
Attn: R. J. Hansen
(Copy No. 16)

Commanding Officer
Naval Underwater Systems Ctr.
Department of the Navy
Newport, RI 02840
Attn: Library
Code 54
(Copy No. 17)

Commanding Officer
Naval Underwater Systems Ctr.
Department of the Navy
Newport, RI 02840
Attn: D. J. Goodrich
Code 3639
(Copy No. 18)

DISTRIBUTION LIST FOR UNCLASSIFIED TECHNICAL MEMORANDUM 85-108, by K. C. Kaufman, dated 25 June 1985 [continuation]

Commanding Officer
Naval Underwater Systems Ctr.
Department of the Navy
Newport, RI 02840
Attn: C. L. Hervey
Code 3634
(Copy No. 19)

Commanding Officer
Naval Underwater Systems Ctr.
Department of the Navy
Newport, RI 02840
Attn: R. H. Nadolink
Code 3634
(Copy No. 20)

Commanding Officer
Naval Underwater Systems Ctr.
Department of the Navy
Newport, RI 02840
Attn: R. B. Phillips
Code 3634
(Copy No. 21)

Office of Naval Research
800 North Quincy Street
Department of the Navy
Arlington, VA 22217
Attn: C. M. Lee
Code 432
(Copy No. 22)

Office of Naval Research
800 North Quincy Street
Department of the Navy
Arlington, VA 22217
Attn: M. M. Reischman
Code 432
(Copy No. 23)

Office of Naval Research
800 North Quincy Street
Department of the Navy
Arlington, VA 22217
Attn: R. E. Whitehead
Code 432
(Copy No. 24)

Director
Applied Research Laboratory
The Pennsylvania State University
Post Office Box 30
State College, PA 16804
Attn: S. A. Abdallah
(Copy No. 25)

Director
Applied Research Laboratory
The Pennsylvania State University
Post Office Box 30
State College, PA 16804
Attn: S. Deutsch
(Copy No. 26)

Director
Applied Research Laboratory
The Pennsylvania State University
Post Office Box 30
State College, PA 16804
Attn: W. R. Hall
(Copy No. 27)

Director
Applied Research Laboratory
The Pennsylvania State University
Post Office Box 30
State College, PA 16804
Attn: L. R. Hettche
(Copy No. 28)

Director
Applied Research Laboratory
The Pennsylvania State University
Post Office Box 30
State College, PA 16804
Attn: G. H. Hoffman
(Copy No. 29)

Director
Applied Research Laboratory
The Pennsylvania State University
Post Office Box 30
State College, PA 16804
Attn: K. C. Kaufman
(Copy No. 30)

DISTRIBUTION LIST FOR UNCLASSIFIED TECHNICAL MEMORANDUM 85-108,
by K. C. Kaufman, dated 25 June 1985 [continuation]

Director
Applied Research Laboratory
The Pennsylvania State University
Post Office Box 30
State College, PA 16804
Attn: B. R. Parkin
(Copy No. 31)

Director
Applied Research Laboratory
The Pennsylvania State University
Post Office Box 30
State College, PA 16804
Attn: GTWT Files
(Copy No. 32)

Director
Applied Research Laboratory
The Pennsylvania State University
Post Office Box 30
State College, PA 16804
Attn: ARL/PSU Library
(Copy No. 33)

# END

# FILMED

10-85

# DTIC